Stress singularities in an anisotropic body of revolution

C.S. Huang, C.N. Hu, C.C. Lee, M.J. Chang *

Department of Civil Engineering, National Chiao Tung University, 1001 Ta-Hsueh Rd., Hsinchu 30050, Taiwan

ABSTRACT

To fill the gap in the literature on the application of three-dimensional elasticity theory to geometrically induced stress singularities, this work develops asymptotic solutions for Williams-type stress singularities in bodies of revolution that are made of rectilinearly anisotropic materials. The Cartesian coordinate system used to describe the material properties differs from the coordinate system used to describe the geometry of a body of revolution, so the problems under consideration are very complicated. The eigenfunction expansion approach is combined with a power series solution technique to find the asymptotic solutions by directly solving the three-dimensional equilibrium equations in terms of the displacement components. The correctness of the proposed solution is verified by convergence studies and by comparisons with results obtained using closed-form characteristic equations for an isotropic body of revolution and using the commercial finite element program ABAQUS for orthotropic bodies of revolution. Thereafter, the solution is employed to comprehensively examine the singularities of bodies of revolution with different geometries, made of a single material or bi-materials, under different boundary conditions.

© 2014 Elsevier Ltd. All rights reserved.

1. Introduction

Many stress singularities caused by material discontinuities and geometric irregularities, such as a notch or an abrupt change in cross-section, occur in real applications. Cracks or damages are commonly initiated at points with stress singularities, so accurately determining the singular behaviors around these singular points is important. Two geometries are frequently considered in investigations of geometrically induced stress singularities: bodies of revolution and wedges. Analytical approaches can be applied to such geometries because of their simplicity. The stress-singular behaviors that are identified for such simple geometries can be utilized to solve stress singularity problems of highly complicated geometries.

The stress singularities in isotropic bodies of revolution or wedges have been comprehensively examined. Since Williams (1952a) pioneered the investigation of stress singularities of plates under extension, many studies of stress singularities in wedges composed of a single material or of multiple materials have been carried out based on the plane strain or stress assumption (e.g., Williams, 1952b; Hein and Erdogan, 1971; England, 1971; Bogy and Wang, 1971; Dempsey and Sinclair, 1981; Ying and Katz, 1987) or three-dimensional elasticity theory (e.g., Hartranft and Sih, 1969; Chaudhuri and Xie, 2000). Geometrically induced stress singularities in plates composed of a single material and of multiple materials have also been extensively studied using classical thin plate theory (e.g., Williams, 1952c; Williams and Owens, 1954), first-order shear deformation plate theory (e.g., Burton and Sinclair, 1986; Huang, 2002a, 2003; Saidi et al., 2010; McGee and Kim, 2005), and third–order plate theory (Huang, 2002b). Only a few investigations of problems involving bodies of revolution have been conducted. Zak (1964) analyzed stresses in the vicinity of boundary discontinuities in the special case of axisymmetric loading. Huang and Leissa (2007) proposed a closed-form asymptotic solution for stress singularities in a body of revolution using three-dimensional theory.

Numerous studies have also been published on geometrically induced stress singularities in an anisotropic body. Most of the literature addresses anisotropic wedge problems because of the wide use of composite materials in engineering applications. Bogy (1972) and Kuo and Bogy (1974) investigated plane traction or displacement problems using the Mellin transform. Assuming that the displacement and stress components were independent of the thickness direction of the wedge, Ting and Chou (1981) adopted the method of Stroh (1962) to determine possible stress distributions close to the vertex of a wedge or a composite wedge of anisotropic materials. Based on the assumption of generalized plane deformation, Chue et al. (2001) and Chue and Liu (2002) determined the singularity orders for composite laminates with an arbitrary fiber orientation using Lekhnitslii's formulation.

Stolarski and Chiang (1989), Pageau et al. (1995), Pageau and Biggers (1996) and Ping et al. (2008) conducted finite element analyses of the stress singularity fields in anisotropic wedges. Applying classical plate theory, Williams and Chapkis (1958) developed the characteristic equations for stress singularities in polarly orthotropic plates, while Ojikutu et al. (1984) analyzed stress singularities in a laminated composite wedge.

No literature is available on geometrically induced stress singularities in an anisotropic body of revolution. The present paper aims to fill the gap by presenting an asymptotic solution for Williams-type stress singularities (i.e., $\sigma_{ij} \propto r^{\lambda}$) in a rectilinearly anisotropic body of revolution, as displayed in Fig. 1, where the $\bar{X}-\bar{Y}-\bar{Z}$ coordinate system is used to describe the material anisotropy whereas the X–Y–Z coordinate system is used to specify the geometry of the body. These two coordinate systems are called the material coordinate system ($\bar{X}-\bar{Y}-\bar{Z}$) and the geometric coordinate system (X–Y–Z). The in-plane displacement components (in the r–Z plane in Fig. 1) are coupled with the out-of-plane displacement component for a general anisotropic body, and the strength of the stress singularity may depend on θ. Unlike solutions for isotropic bodies of revolution, closed-form characteristic equations for the stress singularity orders in a general anisotropic body of revolution cannot be obtained. An eigenfunction expansion approach is combined with a power series method to asymptotically solve the equilibrium equations in terms of the displacements used in three-dimensional elasticity theory. The accuracy of the proposed solution is confirmed by comparing the orders of stress singularities herein with results determined from the characteristic equations for an isotropic body of revolution developed by Huang and Leissa (2007) and obtained from the ABAQUS finite element program for orthotropic bodies of revolution. The presented solution is further applied to examine the effects of boundary conditions, material properties, and the inconsistency between the $\bar{X}-\bar{Y}-\bar{Z}$ and X–Y–Z coordinate systems on the strength of the stress singularities. The present analytical solutions are established based on the general three-dimensional formulation, and can be used to verify solutions that are obtained using numerical techniques, such as finite element approaches.

2. Analysis

Consider an anisotropic body of revolution, shown in Fig. 1, where the $\bar{X}-\bar{Y}-\bar{Z}$ coordinate system is used to describe the
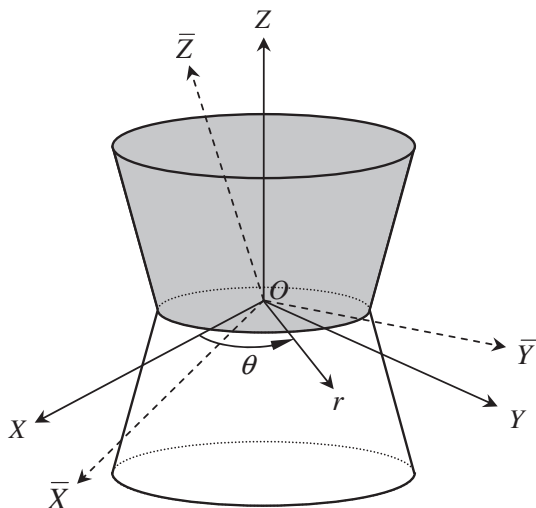

Fig. 1. Bi-material body of revolution with a sharp corner.

material anisotropy and the X–Y–Z coordinate system is used to describe the geometry of the body. The body, subjected to no body forces, should satisfy the following equilibrium equations in terms of the stress components (σ_{ij}) in the cylindrical coordinate system (r, θ, Z) (Fig. 1):

$$\frac{\partial \sigma_{rr}}{\partial r} + \frac{1}{r}\frac{\partial \sigma_{r\theta}}{\partial \theta} + \frac{\partial \sigma_{rz}}{\partial z} + \frac{(\sigma_{rr} - \sigma_{\theta\theta})}{r} = 0, \tag{1a}$$

$$\frac{\partial \sigma_{r\theta}}{\partial r} + \frac{1}{r}\frac{\partial \sigma_{\theta\theta}}{\partial \theta} + \frac{\partial \sigma_{\theta z}}{\partial z} + 2\frac{\sigma_{r\theta}}{r} = 0, \tag{1b}$$

$$\frac{\partial \sigma_{rz}}{\partial r} + \frac{1}{r}\frac{\partial \sigma_{\theta z}}{\partial \theta} + \frac{\partial \sigma_{zz}}{\partial z} + \frac{\sigma_{rz}}{r} = 0. \tag{1c}$$

If the material matrix $[\bar{c}]$ is defined in the $\bar{X}-\bar{Y}-\bar{Z}$ coordinate system, then the relations between the stress components and strain components in the (r, θ, Z) coordinates are

$$\{\sigma\} = [c]\{\varepsilon\}, \tag{2}$$

where

$$\{\sigma\} = \{\begin{matrix} \sigma_{rr} & \sigma_{\theta\theta} & \sigma_{zz} & \sigma_{\theta z} & \sigma_{zr} & \sigma_{r\theta} \end{matrix}\}^T,$$

$$\{\varepsilon\} = \{\begin{matrix} \varepsilon_{rr} & \varepsilon_{\theta\theta} & \varepsilon_{zz} & 2\varepsilon_{\theta z} & 2\varepsilon_{zr} & 2\varepsilon_{r\theta} \end{matrix}\}^T,$$

$$[c] = [T]_\sigma [K][\bar{c}][K]^T [T]_\varepsilon^{-1},$$

$$[T]_\sigma = \begin{bmatrix} \cos^2\theta & \sin^2\theta & 0 & 0 & 0 & 2\cos\theta\sin\theta \\ \sin^2\theta & \cos^2\theta & 0 & 0 & 0 & -2\cos\theta\sin\theta \\ 0 & 0 & 1 & 0 & 0 & 0 \\ 0 & 0 & 0 & \cos\theta & -\sin\theta & 0 \\ 0 & 0 & 0 & \sin\theta & \cos\theta & 0 \\ -\cos\theta\sin\theta & \cos\theta\sin\theta & 0 & 0 & 0 & \cos^2\theta - \sin^2\theta \end{bmatrix},$$

$$[T]_\varepsilon = \begin{bmatrix} \cos^2\theta & \sin^2\theta & 0 & 0 & 0 & \cos\theta\sin\theta \\ \sin^2\theta & \cos^2\theta & 0 & 0 & 0 & -\cos\theta\sin\theta \\ 0 & 0 & 1 & 0 & 0 & 0 \\ 0 & 0 & 0 & \cos\theta & -\sin\theta & 0 \\ 0 & 0 & 0 & \sin\theta & \cos\theta & 0 \\ -2\cos\theta\sin\theta & 2\cos\theta\sin\theta & 0 & 0 & 0 & \cos^2\theta - \sin^2\theta \end{bmatrix},$$

$$[L] = \begin{bmatrix} \cos(\bar{X},X) & \cos(\bar{X},Y) & \cos(\bar{X},Z) \\ \cos(\bar{Y},X) & \cos(\bar{Y},Y) & \cos(\bar{Y},Z) \\ \cos(\bar{Z},X) & \cos(\bar{Z},Y) & \cos(\bar{Z},Z) \end{bmatrix} = \begin{bmatrix} l_{11} & l_{12} & l_{13} \\ l_{21} & l_{22} & l_{23} \\ l_{31} & l_{32} & l_{33} \end{bmatrix},$$

$$[K] = \begin{bmatrix} K_1 & 2K_2 \\ K_3 & K_4 \end{bmatrix}, \quad K_1 = \begin{bmatrix} l_{11}^2 & l_{12}^2 & l_{13}^2 \\ l_{21}^2 & l_{22}^2 & l_{23}^2 \\ l_{31}^2 & l_{32}^2 & l_{33}^2 \end{bmatrix},$$

$$K_2 = \begin{bmatrix} l_{12}l_{13} & l_{13}l_{11} & l_{11}l_{12} \\ l_{22}l_{23} & l_{23}l_{21} & l_{21}l_{22} \\ l_{32}l_{33} & l_{33}l_{31} & l_{31}l_{32} \end{bmatrix},$$

$$K_3 = \begin{bmatrix} l_{21}l_{31} & l_{22}l_{32} & l_{23}l_{33} \\ l_{31}l_{11} & l_{32}l_{12} & l_{33}l_{13} \\ l_{11}l_{21} & l_{12}l_{22} & l_{13}l_{23} \end{bmatrix}, \quad K_4 = \begin{bmatrix} l_{22}l_{33}+l_{23}l_{32} & l_{23}l_{31}+l_{21}l_{33} & l_{21}l_{32}+l_{22}l_{31} \\ l_{32}l_{13}+l_{33}l_{12} & l_{33}l_{11}+l_{31}l_{13} & l_{31}l_{12}+l_{32}l_{11} \\ l_{12}l_{23}+l_{13}l_{22} & l_{13}l_{21}+l_{11}l_{23} & l_{11}l_{22}+l_{12}l_{21} \end{bmatrix}.$$

Hence, the components of $[c]$ are functions of θ and of the angles between the axes of $\bar{X}-\bar{Y}-\bar{Z}$ and X–Y–Z.

Fig. 2 shows a half-plane with a constant θ in Fig. 1. To find an asymptotic solution around the sharp corner in Fig. 2, the (r,Z)
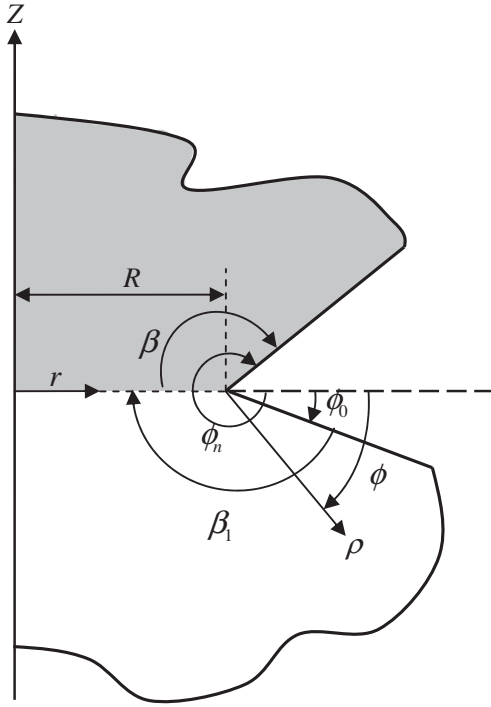
Fig. 2. Cylindrical (r, Z) and sharp corner (ρ, ϕ) coordinates.

coordinates are transformed to (ρ, ϕ) coordinates, as presented in Fig. 2. The relations between (r, Z) and (ρ, ϕ) are

$$\rho = \sqrt{(r-R)^2 + z^2}, \quad \phi = \tan^{-1}\left(\frac{-z}{r-R}\right), \quad r - R$$
$$= \rho\cos\phi, \quad \text{and} \quad z = -\rho\sin\phi. \tag{3}$$

Using the linear relations between the displacements and strains and the relations given in Eq. (3), substituting Eq. (2) into Eq. (1) yields the following equilibrium equations in terms of the displacement components in the (ρ, θ, ϕ) coordinate system:

$$\left\{ (c_{11}L_1 + c_{55}L_3 + 2c_{15}L_5) + \frac{1}{\rho\cos\phi + R}\left[\left(c_{11} + \frac{\partial c_{16}}{\partial\theta}\right)L_2 \right.\right.$$
$$+ \left(c_{15} + \frac{\partial c_{56}}{\partial\theta}\right)L_4 + 2c_{16}\frac{\partial}{\partial\theta}L_2 + 2c_{56}\frac{\partial}{\partial\theta}L_4\bigg]$$
$$\left. + \frac{1}{(\rho\cos\phi + R)^2}\left[-c_{22} + \frac{\partial c_{26}}{\partial\theta} + c_{66}\frac{\partial^2}{\partial\theta^2} + \frac{\partial c_{66}}{\partial\theta}\frac{\partial}{\partial\theta}\right]\right\}u_r$$
$$+ \left\{ (c_{16}L_1 + c_{45}L_3 + (c_{14} + c_{56})L_5) + \frac{1}{\rho\cos\phi + R}\left(-c_{26} + \frac{\partial c_{66}}{\partial\theta}\right)L_2 \right.$$
$$+ \left(c_{14} - c_{24} - c_{56} + \frac{\partial c_{46}}{\partial\theta}\right)L_4 + (c_{12} + c_{66})\frac{\partial}{\partial\theta}L_2 + (c_{25} + c_{46})\frac{\partial}{\partial\theta}L_4$$
$$+ \frac{1}{\rho\cos\phi + R}\left[\left(-c_{26} + \frac{\partial c_{66}}{\partial\theta}\right)L_2 + \left(c_{14} - c_{24} - c_{56} + \frac{\partial c_{46}}{\partial\theta}\right)L_4\right]$$
$$\left. + \frac{1}{(\rho\cos\phi + R)^2}\left[c_{26} - \frac{\partial c_{66}}{\partial\theta} + c_{26}\frac{\partial^2}{\partial\theta^2} + \left(-c_{22} - c_{66} + \frac{\partial c_{26}}{\partial\theta}\right)\frac{\partial}{\partial\theta}\right]\right\}u_\theta$$
$$+ \left\{ (c_{15}L_1 + c_{35}L_3 + (c_{13} + c_{55})L_5) + \frac{1}{\rho\cos\phi + R}\left[\left(c_{15} - c_{25} + \frac{\partial c_{56}}{\partial\theta}\right)L_2 \right.\right.$$
$$+ \left(c_{13} - c_{23} + \frac{\partial c_{36}}{\partial\theta}\right)L_4 + (c_{14} + c_{56})\frac{\partial}{\partial\theta}L_2 + (c_{36} + c_{45})\frac{\partial}{\partial\theta}L_4\bigg]$$
$$\left. + \frac{1}{(\rho\cos\phi + R)^2}\left[\left(-c_{24} + \frac{\partial c_{46}}{\partial\theta}\right)\frac{\partial}{\partial\theta} + c_{46}\frac{\partial^2}{\partial\theta^2}\right]\right\}u_z = 0, \tag{4a}$$

$$\left\{ (c_{16}L_1 + c_{45}L_3 + (c_{56} + c_{14})L_5) + \frac{1}{\rho\cos\phi + R}\left[\left(2c_{16} + c_{26} + \frac{\partial c_{12}}{\partial\theta}\right)L_2 \right.\right.$$
$$+ \left(2c_{56} + c_{24} + \frac{\partial c_{25}}{\partial\theta}\right)L_4 + (c_{21} + c_{66})\frac{\partial}{\partial\theta}L_2 + (c_{25} + c_{46})\frac{\partial}{\partial\theta}L_4\bigg]$$
$$\left. + \frac{1}{(\rho\cos\phi + R)^2}\left[\left(c_{26} + \frac{\partial c_{22}}{\partial\theta} + c_{26}\frac{\partial^2}{\partial\theta^2}\right) + \left(c_{22} + c_{66} + \frac{\partial c_{26}}{\partial\theta}\right)\frac{\partial}{\partial\theta}\right]\right\}u_r$$
$$+ \left\{ (c_{66}L_1 + c_{44}L_3 + 2c_{46}L_5) + \frac{1}{\rho\cos\phi + R}\left[\left(c_{66} + \frac{\partial c_{26}}{\partial\theta}\right)L_2 \right.\right.$$
$$+ \left(c_{46} + \frac{\partial c_{24}}{\partial\theta}\right)L_4 + 2c_{26}\frac{\partial}{\partial\theta}L_2 + 2c_{24}\frac{\partial}{\partial\theta}L_4\bigg]$$
$$\left. + \frac{1}{(\rho\cos\phi + R)^2}\left[\left(\frac{\partial c_{22}}{\partial\theta}\right)\frac{\partial}{\partial\theta} + \left(-c_{66} - \frac{\partial c_{26}}{\partial\theta} + c_{22}\frac{\partial^2}{\partial\theta^2}\right)\right]\right\}u_\theta$$
$$+ \left\{ (c_{56}L_1 + c_{34}L_3 + (c_{36} + c_{45})L_5) + \frac{1}{\rho\cos\phi + R}\left[\left(2c_{56} + \frac{\partial c_{25}}{\partial\theta}\right)L_2 \right.\right.$$
$$+ \left(2c_{36} + \frac{\partial c_{23}}{\partial\theta}\right)L_4 + (c_{25} + c_{46})\frac{\partial}{\partial\theta}L_2 + (c_{23} + c_{44})\frac{\partial}{\partial\theta}L_4\bigg]$$
$$\left. + \frac{1}{(\rho\cos\phi + R)^2}\left[\left(c_{46} + \frac{\partial c_{24}}{\partial\theta}\right)\frac{\partial}{\partial\theta} + c_{24}\frac{\partial^2}{\partial\theta^2}\right]\right\}u_z = 0, \tag{4b}$$

$$\left\{ (c_{15}L_1 + c_{35}L_3 + (c_{55} + c_{13})L_5) + \frac{1}{\rho\cos\phi + R}\left[\left(c_{15} + c_{25} + \frac{\partial c_{14}}{\partial\theta}\right)L_2 \right.\right.$$
$$+ \left(c_{23} + c_{55} + \frac{\partial c_{45}}{\partial\theta}\right)L_4 + (c_{14} + c_{56})\frac{\partial}{\partial\theta}L_2 + (c_{45} + c_{36})\frac{\partial}{\partial\theta}L_4\bigg]$$
$$\left. + \frac{1}{(\rho\cos\phi + R)^2}\left[\left(\frac{\partial c_{24}}{\partial\theta} + c_{46}\frac{\partial^2}{\partial\theta^2}\right) + \left(c_{24} + \frac{\partial c_{46}}{\partial\theta}\right)\frac{\partial}{\partial\theta}\right]\right\}u_r$$
$$+ \left\{ (c_{56}L_1 + c_{34}L_3 + (c_{45} + c_{36})L_5) + \frac{1}{\rho\cos\phi + R}\left[\left(\frac{\partial c_{46}}{\partial\theta}\right)L_2 \right.\right.$$
$$+ \left(c_{45} - c_{36} + \frac{\partial c_{44}}{\partial\theta}\right)L_4 + (c_{25} + c_{46})\frac{\partial}{\partial\theta}L_2 + (c_{44} + c_{23})\frac{\partial}{\partial\theta}L_4\bigg]$$
$$\left. + \frac{1}{(\rho\cos\phi + R)^2}\left[\left(-c_{46} + \frac{\partial c_{24}}{\partial\theta}\right)\frac{\partial}{\partial\theta} + \left(-\frac{\partial c_{46}}{\partial\theta} + c_{24}\frac{\partial^2}{\partial\theta^2}\right)\right]\right\}u_\theta$$
$$+ \left\{ (c_{55}L_1 + c_{33}L_3 + 2c_{35}L_5) + \frac{1}{\rho\cos\phi + R}\left[\left(c_{55} + \frac{\partial c_{45}}{\partial\theta}\right)L_2 \right.\right.$$
$$+ \left(c_{35} + \frac{\partial c_{34}}{\partial\theta}\right)L_4 + 2c_{45}\frac{\partial}{\partial\theta}L_2 + 2c_{34}\frac{\partial}{\partial\theta}L_4\bigg]$$
$$\left. + \frac{1}{(\rho\cos\phi + R)^2}\left[\left(\frac{\partial c_{44}}{\partial\theta}\right)\frac{\partial}{\partial\theta} + c_{44}\frac{\partial^2}{\partial\theta^2}\right]\right\}u_z = 0, \tag{4c}$$

where u_r, u_θ, and u_z are the displacement components in the r, θ, and Z directions, respectively; c_{ij} is the (i,j) component in $[c]$; and

$$L_1 = \cos^2\phi\frac{\partial^2}{\partial\rho^2} + \frac{\sin^2\phi}{\rho}\frac{\partial}{\partial\rho} - \frac{2\sin\phi\cos\phi}{\rho}\frac{\partial^2}{\partial\rho\partial\phi} + \frac{2\sin\phi\cos\phi}{\rho^2}\frac{\partial}{\partial\phi}$$
$$+ \frac{\sin^2\phi}{\rho^2}\frac{\partial^2}{\partial\phi^2},$$

$$L_2 = \cos\phi\frac{\partial}{\partial\rho} - \frac{\sin\phi}{\rho}\frac{\partial}{\partial\phi},$$

$$L_3 = \sin^2\phi\frac{\partial^2}{\partial\rho^2} + \frac{\cos^2\phi}{\rho}\frac{\partial}{\partial\rho} + \frac{2\sin\phi\cos\phi}{\rho}\frac{\partial^2}{\partial\rho\partial\phi} - \frac{2\sin\phi\cos\phi}{\rho^2}\frac{\partial}{\partial\phi}$$
$$+ \frac{\cos^2\phi}{\rho^2}\frac{\partial^2}{\partial\phi^2},$$

$$L_4 = \frac{\partial}{\partial\rho}\frac{\partial\rho}{\partial z} + \frac{\partial}{\partial\phi}\frac{\partial\phi}{\partial z} = -\sin\phi\frac{\partial}{\partial\rho} - \frac{\cos\phi}{\rho}\frac{\partial}{\partial\phi},$$

$$L_5 = -\sin\phi\cos\phi\frac{\partial^2}{\partial\rho^2} + \frac{\sin\phi\cos\phi}{\rho}\frac{\partial}{\partial\rho} - \frac{\cos2\phi}{\rho}\frac{\partial^2}{\partial\rho\partial\phi} + \frac{\cos2\phi}{\rho^2}\frac{\partial}{\partial\phi}$$
$$+ \frac{\sin\phi\cos\phi}{\rho^2}\frac{\partial^2}{\partial\phi^2}.$$

Eq. (4) are complicated partial differential equations with variable coefficients. The eigenfunction expansion approach used by Hartranft and Sih (1969) for an isotropic wedge is utilized herein to establish an asymptotic solution around the sharp corner in Fig. 2. We assume

$$u_r(\rho,\theta,\phi) = \sum_{m=1}^{\infty}\sum_{n=0}^{\infty}\rho^{\lambda_m+n}\hat{U}_n^{(m)}(\theta,\phi),$$

$$u_\theta(\rho,\theta,\phi) = \sum_{m=1}^{\infty}\sum_{n=0}^{\infty}\rho^{\lambda_m+n}\hat{V}_n^{(m)}(\theta,\phi),$$

$$u_z(\rho,\theta,\phi) = \sum_{m=1}^{\infty}\sum_{n=0}^{\infty}\rho^{\lambda_m+n}\hat{W}_n^{(m)}(\theta,\phi), \tag{5}$$

where λ_m can be a sequence of complex numbers, ordered $\mathrm{Re}[\lambda_i] \leqslant \mathrm{Re}[\lambda_{i+1}]$, whose real part must be positive to ensure finite displacements at $\rho = 0$. Substituting Eq. (5) into Eq. (4) and considering the terms in the least power of ρ yields

$$\frac{\partial^2\hat{U}_0^{(m)}}{\partial\phi^2} + \frac{1}{\Delta_1}(\lambda_m-1)[(c_{55}-c_{11})\sin2\phi - 2c_{15}\cos2\phi]\frac{\partial\hat{U}_0^{(m)}}{\partial\phi}$$
$$+ \frac{1}{\Delta_1}\Big[\lambda_m((\lambda_m-1)c_{55}+c_{11})\sin^2\phi + \lambda_m((\lambda_m-1)c_{11}+c_{55})\cos^2\phi$$
$$+ \lambda_m(2-\lambda_m)c_{15}\sin2\phi]\hat{U}_0^{(m)} + \frac{1}{\Delta_1}\Big\{\Big[c_{16}\sin^2\phi + c_{45}\cos^2\phi$$
$$+ \frac{(c_{14}+c_{56})}{2}\sin2\phi\Big]\frac{\partial^2\hat{V}_0^{(m)}}{\partial\phi^2} + (\lambda_m-1)[(c_{45}-c_{16})\sin2\phi$$
$$- \Big(c_{14}+c_{56}\Big)\cos2\phi]\frac{\partial\hat{V}_0^{(m)}}{\partial\phi} + \Big[\lambda_m(\lambda_m-1)(c_{16}\cos^2\phi + c_{45}\sin^2\phi$$
$$- \frac{(c_{14}+c_{56})}{2}\sin2\phi)\lambda_m\Big(c_{16}\sin^2\phi + c_{45}\cos^2\phi + \frac{(c_{14}+c_{56})}{2}\sin2\phi\Big)\Big]\hat{V}_0^{(m)}\Big\}$$
$$+ \frac{1}{\Delta_1}\Big\{\Big[c_{15}\sin^2\phi + c_{35}\cos^2\phi + \frac{(c_{13}+c_{55})}{2}\sin2\phi\Big]\frac{\partial^2\hat{W}_0^{(m)}}{\partial\phi^2}$$
$$+ (\lambda_m-1)[(c_{35}-c_{15})\sin2\phi - (c_{13}+c_{55})\cos2\phi]\frac{\partial\hat{W}_0^{(m)}}{\partial\phi}$$
$$+ \Big[\lambda_m(\lambda_m-1)\Big(c_{15}\cos^2\phi + c_{35}\sin^2\phi - \frac{(c_{13}+c_{55})}{2}\sin2\phi\Big)$$
$$+ \lambda_m\Big(c_{15}\sin^2\phi + c_{35}\cos^2\phi + \frac{(c_{13}+c_{55})}{2}\sin2\phi\Big)\Big]\hat{W}_0^{(m)}\Big\} = 0, \tag{6a}$$

$$\frac{\partial^2\hat{V}_0^{(m)}}{\partial\phi^2} + \frac{1}{\Delta_2}(\lambda_m-1)[(c_{44}-c_{66})\sin2\phi - 2c_{46}\cos2\phi]\frac{\partial\hat{V}_0^{(m)}}{\partial\phi}$$
$$+ \frac{1}{\Delta_2}\Big[\lambda_m((\lambda_m-1)c_{44}+c_{66})\sin^2\phi + \lambda_m((\lambda_m-1)c_{66}+c_{44})\cos^2\phi$$
$$+ \lambda_m(2-\lambda_m)c_{46}\sin2\phi\Big]\hat{V}_0^{(m)} + \frac{1}{\Delta_2}\Big\{\Big[c_{16}\sin^2\phi + c_{45}\cos^2\phi$$
$$+ \frac{(c_{56}+c_{14})}{2}\sin2\phi\Big]\frac{\partial^2\hat{U}_0^{(m)}}{\partial\phi^2}(\lambda_m-1)[(c_{45}-c_{16})\sin2\phi$$
$$- (c_{56}+c_{14})\cos2\phi]\frac{\partial\hat{U}_0^{(m)}}{\partial\phi}\Big[\lambda_m(\lambda_m-1)(c_{16}\cos^2\phi + c_{45}\sin^2\phi$$
$$- \frac{(c_{56}+c_{14})}{2}\sin2\phi) + \lambda_m(c_{16}\sin^2\phi + c_{45}\cos^2\phi$$
$$+ \frac{(c_{56}+c_{14})}{2}\sin2\phi)\Big]\hat{U}_0^{(m)}\Big\}$$

$$+ \frac{1}{\Delta_2}\Big\{\Big[c_{56}\sin^2\phi + c_{34}\cos^2\phi + \frac{(c_{36}+c_{45})}{2}\sin2\phi\Big]\frac{\partial^2\hat{W}_0^{(m)}}{\partial\phi^2}$$
$$+ (\lambda_m-1)[(c_{34}-c_{56})\sin2\phi - (c_{36}+c_{45})\cos2\phi]\frac{\partial\hat{W}_0^{(m)}}{\partial\phi}$$
$$+ \Big[\lambda_m(\lambda_m-1)(c_{56}\cos^2\phi + c_{34}\sin^2\phi - \frac{(c_{36}+c_{45})}{2}\sin2\phi)$$
$$+ \lambda_m\Big(c_{56}\sin^2\phi + c_{34}\cos^2\phi + \frac{(c_{36}+c_{45})}{2}\sin2\phi\Big)\Big]\hat{W}_0^{(m)}\Big\} = 0, \tag{6b}$$

$$\frac{\partial^2\hat{W}_0^{(m)}}{\partial\phi^2} + \frac{1}{\Delta_3}(\lambda_m-1)[(c_{33}-c_{55})\sin2\phi - 2c_{35}\cos2\phi]\frac{\partial\hat{W}_0^{(m)}}{\partial\phi}$$
$$+ \frac{1}{\Delta_3}\Big[\lambda_m((\lambda_m-1)c_{33}+c_{55})\sin^2\phi + \lambda_m((\lambda_m-1)c_{55}+c_{33})\cos^2\phi$$
$$+ \lambda_m(2-\lambda_m)c_{35}\sin2\phi\Big]\hat{W}_0^{(m)}$$
$$+ \frac{1}{\Delta_3}\Big\{\Big[c_{15}\sin^2\phi + c_{35}\cos^2\phi + \frac{(c_{13}+c_{55})}{2}\sin2\phi\Big]\frac{\partial^2\hat{U}_0^{(m)}}{\partial\phi^2}$$
$$+ (\lambda_m-1)[(c_{35}-c_{15})\sin2\phi - (c_{13}+c_{55})\cos2\phi]\frac{\partial\hat{U}_0^{(m)}}{\partial\phi}$$
$$\times \Big[\lambda_m(\lambda_m-1)(c_{15}\cos^2\phi + c_{35}\sin^2\phi - \frac{(c_{13}+c_{55})}{2}\sin2\phi)$$
$$+ \lambda_m(c_{15}\sin^2\phi + c_{35}\cos^2\phi + \frac{(c_{31}+c_{55})}{2}\sin2\phi)\Big]\hat{U}_0^{(m)}\Big\}$$
$$+ \frac{1}{\Delta_3}\Big\{\Big[c_{56}\sin^2\phi + c_{34}\cos^2\phi + \frac{(c_{36}+c_{45})}{2}\sin2\phi\Big]\frac{\partial^2\hat{V}_0^{(m)}}{\partial\phi^2}$$
$$+ (\lambda_m-1)[(c_{34}-c_{56})\sin2\phi - (c_{36}+c_{45})\cos2\phi]\frac{\partial\hat{V}_0^{(m)}}{\partial\phi}$$
$$+ \Big[\lambda_m(\lambda_m-1)\Big(c_{56}\cos^2\phi + c_{34}\sin^2\phi - \frac{(c_{36}+c_{45})}{2}\sin2\phi\Big)$$
$$+ \lambda_m\Big(c_{56}\sin^2\phi + c_{34}\cos^2\phi + \frac{(c_{36}+c_{45})}{2}\sin2\phi\Big)\Big]\hat{V}_0^{(m)}\Big\} = 0, \tag{6c}$$
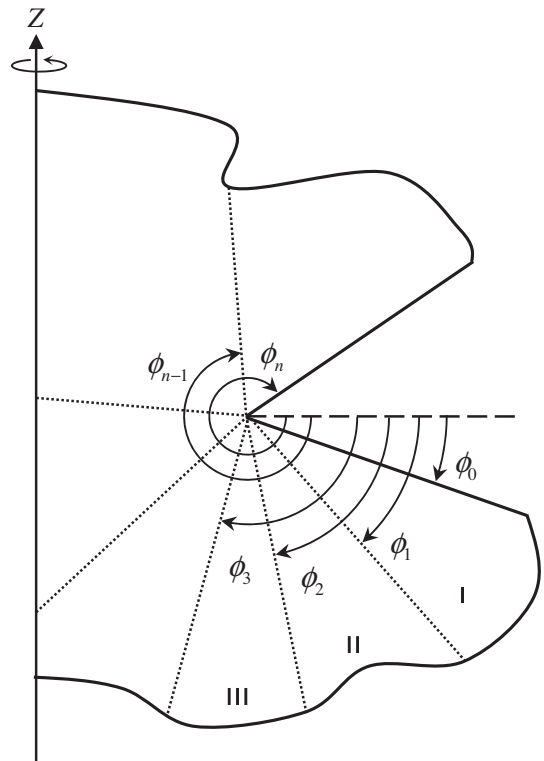

Fig. 3. Sub-domains for $\phi \in [\phi_0, \phi_n]$.

where $\quad \Delta_1 = c_{11}\sin^2\phi + c_{55}\cos^2\phi + c_{15}\sin^2\phi, \quad \Delta_2 = c_{66}\sin^2\phi + c_{44}\cos^2\phi + c_{46}\sin^2\phi$, and $\Delta_3 = c_{55}\sin^2\phi + c_{33}\cos^2\phi + c_{35}\sin^2\phi$.

Eq. (6) is a set of ordinary differential equations with variable coefficients that depend on θ and ϕ. The three displacement components are coupled. The exact closed-form solutions to Eq. (6) are intractable, if they exist. The power series method can be directly adopted to develop a general solution to the ordinary differential equations. Very high-order terms are often needed to obtain an accurate solution and usually cause numerical difficulties. To overcome these difficulties, a domain decomposition technique is applied in conjunction with the power series method to establish a general solution to Eq. (6).

The range of ϕ under consideration is first divided into a number of sub-domains (Fig. 3). A series solution to Eq. (6) is constructed in each sub-domain. Consequently, a general solution over the whole ϕ domain is obtained by assembling the solutions in all sub-domains and imposing continuity conditions between each pair of adjacent sub-domains. This process is a very convenient means of constructing solutions for multi-material bodies of revolution, which are also considered in this work.

To establish the power series solution for sub-domain i of ϕ, the variable coefficients in Eq. (6) are expanded in terms of the power series of ϕ with respect to the middle point of the sub-domain $\bar{\phi}_i$:

$$
\begin{aligned}
&\frac{\sin 2\phi}{\Delta_1} = \sum_{k=0}^{K} a_k^{(i)}(\phi - \bar{\phi}_i)^k, \quad \frac{\cos^2\phi}{\Delta_1} = \sum_{k=0}^{K} b_k^{(i)}(\phi - \bar{\phi}_i)^k, \\
&\frac{\sin^2\phi}{\Delta_1} = \sum_{k=0}^{K} c_k^{(i)}(\phi - \bar{\phi}_i)^k, \\
&\frac{\cos 2\phi}{\Delta_1} = \sum_{k=0}^{K} d_k^{(i)}(\phi - \bar{\phi}_i)^k, \quad \frac{\sin 2\phi}{\Delta_2} = \sum_{k=0}^{K} e_k^{(i)}(\phi - \bar{\phi}_i)^k, \\
&\frac{\cos^2\phi}{\Delta_2} = \sum_{k=0}^{K} f_k^{(i)}(\phi - \bar{\phi}_i)^k, \\
&\frac{\sin^2\phi}{\Delta_2} = \sum_{k=0}^{K} g_k^{(i)}(\phi - \bar{\phi}_i)^k, \quad \frac{\cos 2\phi}{\Delta_2} = \sum_{k=0}^{K} h_k^{(i)}(\phi - \bar{\phi}_i)^k, \\
&\frac{\sin 2\phi}{\Delta_3} = \sum_{k=0}^{K} l_k^{(i)}(\phi - \bar{\phi}_i)^k, \\
&\frac{\cos^2\phi}{\Delta_3} = \sum_{k=0}^{K} m_k^{(i)}(\phi - \bar{\phi}_i)^k, \quad \frac{\sin^2\phi}{\Delta_3} = \sum_{k=0}^{K} n_k^{(i)}(\phi - \bar{\phi}_i)^k, \\
&\frac{\cos 2\phi}{\Delta_3} = \sum_{k=0}^{K} o_k^{(i)}(\phi - \bar{\phi}_i)^k.
\end{aligned}
\tag{7}
$$

Table 1
Material properties of orthotropic materials.

Stiffness (GPa)	Material		
	TiSi$_2$	BaSO$_4$	FeSiO$_3$
$\bar{c}_{11}$	377.2	89.4	198.0
$\bar{c}_{12}$	27.8	46.1	84.0
$\bar{c}_{13}$	21.3	26.9	72.0
$\bar{c}_{14}$	0.0	0.0	0.0
$\bar{c}_{15}$	0.0	0.0	0.0
$\bar{c}_{16}$	0.0	0.0	0.0
$\bar{c}_{22}$	341.1	78.4	136.0
$\bar{c}_{23}$	95.1	26.7	55.0
$\bar{c}_{24}$	0.0	0.0	0.0
$\bar{c}_{25}$	0.0	0.0	0.0
$\bar{c}_{26}$	0.0	0.0	0.0
$\bar{c}_{33}$	425.3	105.4	175.0
$\bar{c}_{34}$	0.0	0.0	0.0
$\bar{c}_{35}$	0.0	0.0	0.0
$\bar{c}_{36}$	0.0	0.0	0.0
$\bar{c}_{44}$	136.5	11.9	59.0
$\bar{c}_{45}$	0.0	0.0	0.0
$\bar{c}_{46}$	0.0	0.0	0.0
$\bar{c}_{55}$	93.7	28.7	58.0
$\bar{c}_{56}$	0.0	0.0	0.0
$\bar{c}_{66}$	154.6	27.7	49.0

Table 2
Convergence study of λ_1 for an isotropic body of revolution with $\alpha = 270°$.
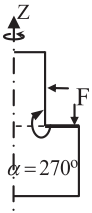
Geometry/boundary condition	Number of sub-domains	Number of polynomial terms					Huang and Leissa (2007)
		2	4	8	12	16	
	2	0.5274	0.5246	0.5442	0.5445	0.5445	0.5445
	4	0.5517	0.5439	0.5445	0.5445	0.5445	
	8	0.5468	0.5444	0.5445	0.5445	0.5445	
	10	0.5456	0.5445	0.5445	0.5445	0.5445	

Table 3
Convergence study of λ_1 for an orthotropic body of revolution with $\alpha = 360°$.
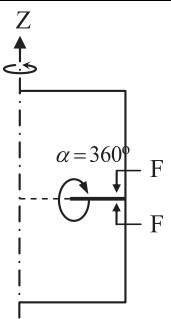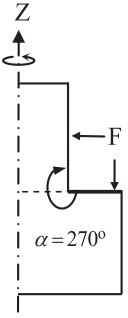
Geometry/boundary condition	Cases	Number of sub-domains	Number of polynomial terms					ABAQUS
			2	4	8	12	16	
	1	2	0.4201	0.4359	0.4995	0.5000	0.5000	0.5001
		4	0.4141	0.4466	0.5000	0.5000	0.4999	
		8	0.4631	0.4993	0.4998	0.4999	0.5000	
		10	0.4918	0.4999	0.4999	0.4999	0.5000	
	2	2	0.3933	0.4566	0.4842	0.5140	0.5123	0.4999
		4	0.4191	0.4557	0.4961	0.5014	0.4984	
		8	0.4902	0.4990	0.4998	0.4999	0.4999	
		10	0.4930	0.4999	0.4999	0.4999	0.5000	

Table 4
Convergence study of λ_1 for an orthotropic body of revolution with $\alpha = 270°$.

Geometry/boundary condition	Cases	Number of sub-domains	Number of polynomial terms					ABAQUS
			2	4	8	12	16	
	1	2	0.6532	0.6479	0.6665	0.6553	0.6424	0.5500
		4	0.5575	0.5538	0.5500	0.5506	0.5500	
		8	0.5564	0.5511	0.5501	0.5502	0.5502	
		10	0.5521	0.5500	0.5502	0.5502	0.5502	
	2	2	0.5964	0.6671	0.6068	0.5992	0.5905	0.5461
		4	0.5770	0.5504	0.5546	0.5595	0.5606	
		8	0.5561	0.5439	0.5461	0.5463	0.5463	
		10	0.5496	0.5452	0.5463	0.5463	0.5463	

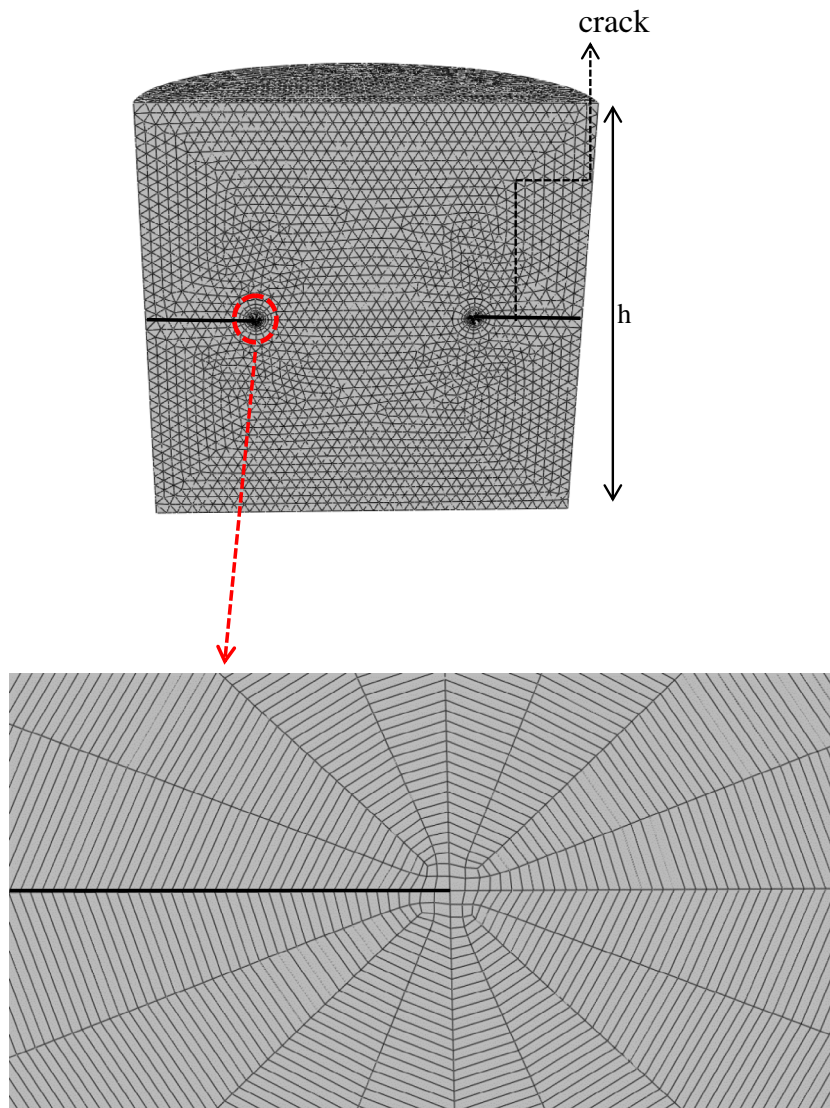**Fig. 4.** A finite element model and mesh configuration.

Similarly, the solutions to Eq. (6) in sub-domain i are expressed as

$$\hat{U}_{0i}^{(m)} = \sum_{j=0}^{J} \hat{A}_j^{(im)}(\phi - \bar{\phi}_i)^j, \quad \hat{V}_{0i}^{(m)} = \sum_{j=0}^{J} \hat{B}_j^{(im)}(\phi - \bar{\phi}_i)^j,$$

$$\hat{W}_{0i}^{(m)} = \sum_{j=0}^{J} \hat{C}_j^{(im)}(\phi - \bar{\phi}_i)^j. \tag{8}$$

Substituting Eqs. (7) and (8) into Eq. (6) and carefully rearranging the terms yields the following recurrence relations among the unknown coefficients in Eq. (8):

$$\hat{A}_{j+2}^{(im)} + \left(c_{16}c_0 + c_{45}b_0 + \frac{(c_{14}+c_{56})}{2}a_0 \right)\hat{B}_{j+2}^{(im)}$$

$$+ \left(c_{15}c_0 + c_{35}b_0 + \frac{(c_{13}+c_{55})}{2}a_0 \right)\hat{C}_{j+2}^{(im)}$$

$$= \frac{-1}{(j+2)(j+1)}\left\{ \sum_{k=0}^{j-1}\left(c_{16}c_{j-k} + c_{45}b_{j-k} + \frac{(c_{14}+c_{56})}{2}a_{j-k} \right) \right.$$

$$\times (k+2)(k+1)\hat{B}_{k+2}^{(im)} + \left(c_{15}c_{j-k} + c_{35}b_{j-k} + \frac{(c_{13}+c_{55})}{2}a_{j-k} \right)$$

$$\times (k+2)(k+1)\hat{C}_{k+2}^{(im)} + \sum_{k=0}^{j}(\lambda_m - 1)[(c_{55}-c_{11})a_{j-k} - 2c_{15}d_{j-k}]$$

$$\times (k+1)\hat{A}_k^{(im)} + [\lambda_m((\lambda_m-1)c_{55}+c_{11})c_{j-k} + \lambda_m((\lambda_m-1)c_{11}+c_{55})b_{j-k}$$

$$+ \lambda(2-\lambda)c_{15}a_{j-k}]\hat{A}_k^{(im)} + (\lambda_m-1)[(c_{45}-c_{16})a_{j-k}$$

$$- (c_{14}+c_{56})d_{j-k}](k+1)\hat{B}_{k+1}^{(im)}$$

$$+ \left[\lambda_m(\lambda_m-1) \times \left(c_{16}b_{j-k} + c_{45}c_{j-k} - \frac{(c_{14}+c_{56})}{2}a_{j-k} \right) \right.$$

$$+ \lambda_m\left(c_{16}c_{j-k} + c_{45}b_{j-k} + \frac{(c_{14}+c_{56})}{2}a_{j-k} \right)\right]\hat{B}_k^{(im)}$$

$$+ (\lambda_m-1)[(c_{35}-c_{15})a_{j-k} - (c_{13}+c_{55})d_{j-k}](k+1)\hat{C}_{k+1}^{(im)}$$

$$+ \left[\lambda_m(\lambda_m-1) \times \left(c_{15}b_{j-k} + c_{35}c_{j-k} - \frac{(c_{13}+c_{55})}{2}a_{j-k} \right) \right.$$

$$+ \lambda_m\left(c_{15}c_{j-k} + c_{35}b_{j-k} + \frac{(c_{13}+c_{55})}{2}a_{j-k} \right)\left]\hat{C}_k^{(im)} \right\}, \tag{9a}$$

$$\hat{B}_{j+2}^{(im)} + \left(c_{16}g_0 + c_{45}f_0 + \frac{(c_{56}+c_{14})}{2}e_0 \right)\hat{A}_{j+2}^{(im)}$$

$$+ \left(c_{56}g_0 + c_{34}f_0 + \frac{(c_{36}+c_{45})}{2}e_0 \right)\hat{C}_{j+2}^{(im)}$$

$$= \frac{-1}{(j+2)(j+1)}\left\{ \sum_{k=0}^{j-1}\left(c_{16}g_{j-k} + c_{45}f_{j-k} + \frac{(c_{56}+c_{14})}{2}e_{j-k} \right) \right.$$

$$\times (+2)(k+1)\hat{A}_{k+2}^{(im)} + \left(c_{56}g_{j-k} + c_{34}f_{j-k} + \frac{(c_{36}+c_{45})}{2}e_{j-k} \right)$$

$$\times (+2)(k+1)\hat{C}_{k+2}^{(im)} + \sum_{k=0}^{j}(\lambda_m-1)[(c_{44}-c_{66})e_{j-k} - 2c_{46}h_{j-k}](k+1)\hat{B}_{k+1}^{(im)}$$

$$+ [\lambda_m((\lambda_m-1)c_{44}+c_{66})g_{j-k} + \lambda_m((\lambda_m-1)c_{66}+c_{44})f_{j-k}$$

$$+ \lambda_m(2-\lambda_m)c_{45}e_{j-k}]\hat{B}_k^{(im)} + (\lambda_m-1)[(c_{45}-c_{16})e_{j-k}$$

$$- (c_{56}+c_{14})h_{j-k}](k+1)\hat{A}_{k+1}^{(im)} + \left[\lambda_m(\lambda_m-1) \right.$$

$$\times \left(c_{16}f_{j-k} + c_{45}g_{j-k} - \frac{(c_{56}+c_{14})}{2}e_{j-k} \right)$$

$$+ \lambda_m\left(c_{16}g_{j-k} + c_{45}f_{j-k} + \frac{(c_{56}+c_{14})}{2}e_{j-k} \right)\right]\hat{A}_k^{(im)}$$

$$+ (\lambda_m-1)[(c_{34}-c_{56})e_{j-k} - (c_{36}+c_{45})h_{j-k}](k+1)\hat{C}_{k+1}^{(im)}$$

$$+ \left[\lambda_m(\lambda_m-1) \times (c_{56}f_{j-k} + c_{34}g_{j-k} - \frac{(c_{36}+c_{45})}{2}e_{j-k}) \right.$$

$$+ \lambda_m\left(c_{56}g_{j-k} + c_{34}f_{j-k} + \frac{(c_{36}+c_{45})}{2}e_{j-k} \right)\left]\hat{C}_k^{(im)} \right\}, \tag{9b}$$
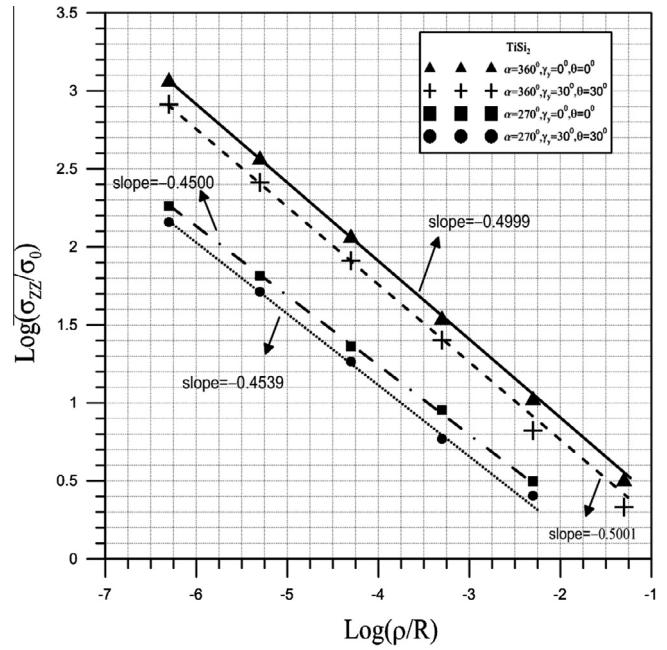
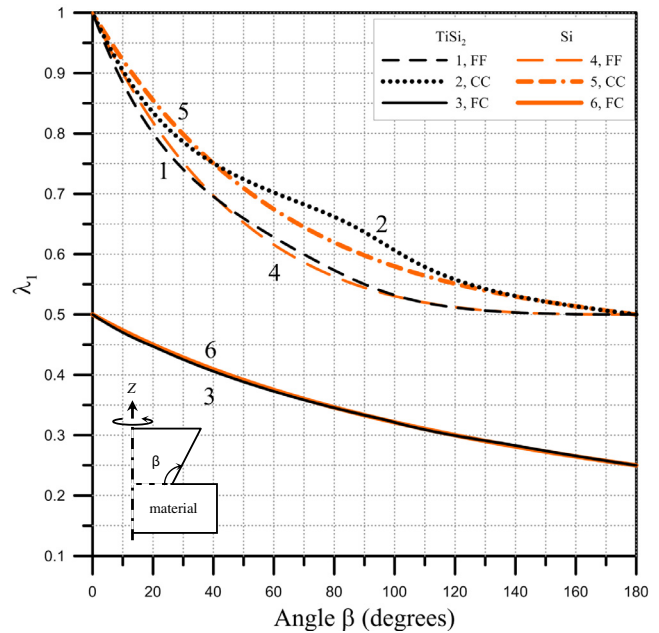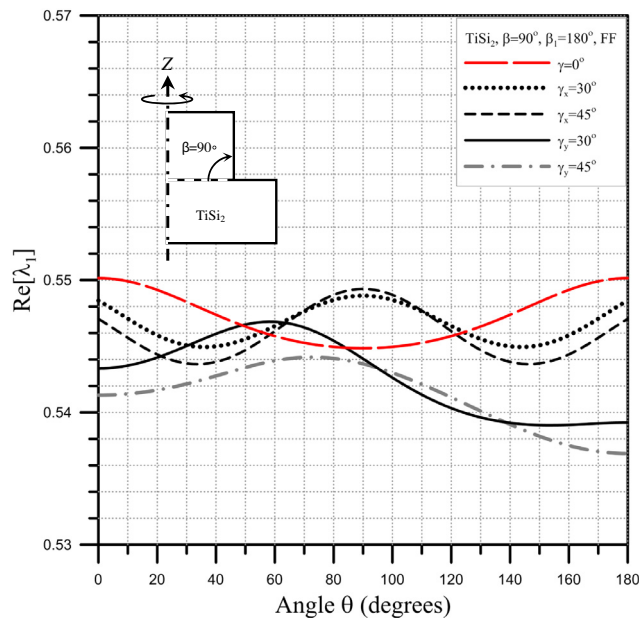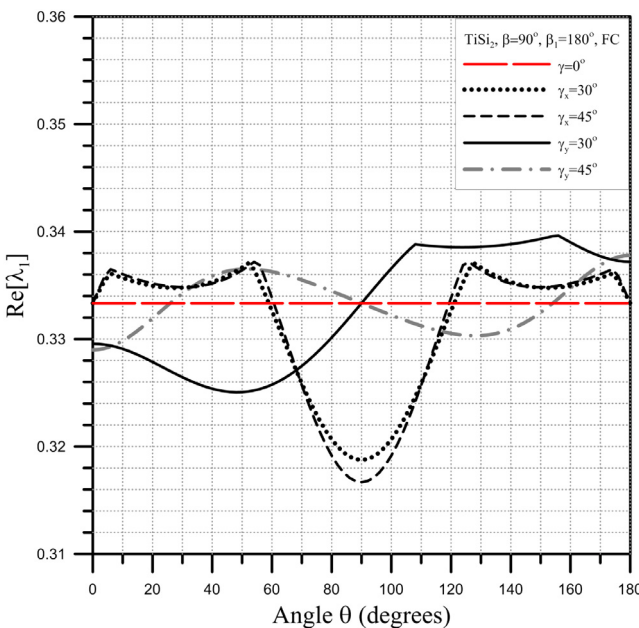Fig. 5. Variation of σ_{zz} with respect to ρ/R.

Fig. 6. Variation of λ_1 at $\theta = 0°$ with respect to β for TiSi$_2$ and Si bodies of revolution having $\beta_1 = 180°$ under FF, FC, and CC boundary conditions.

$$\hat{C}_{j+2}^{(im)} + \left(c_{15}n_0 + c_{35}m_0 + \frac{(c_{13}+c_{55})}{2}l_0 \right)\hat{A}_{j+2}^{(im)}$$

$$+ \left(c_{56}n_0 + c_{34}m_0 + \frac{(c_{36}+c_{45})}{2}l_0 \right)\hat{B}_{j+2}^{(im)}$$

$$= \frac{-1}{(j+2)(j+1)}\left\{ \sum_{k=0}^{j-1}\left(c_{15}n_{j-k} + c_{35}m_{j-k} + \frac{(c_{13}+c_{55})}{2}l_{j-k} \right) \right.$$

$$\times (+2)(k+1)\hat{A}_{k+2}^{(im)} + \left(c_{56}n_{j-k} + c_{34}m_{j-k} + \frac{(c_{36}+c_{45})}{2}l_{j-k} \right)$$

$$\times (+2)(k+1)\hat{B}_{k+2}^{(im)} + \sum_{k=0}^{j}(\lambda_m-1)[(c_{33}-c_{55})l_{j-k} - 2c_{35}o_{j-k}]$$

$$\times (+1)\hat{C}_{k+1}^{(im)} + [\lambda_m((\lambda_m - 1)c_{33} + c_{55})n_{j-k}$$
$$+\lambda_m((\lambda_m - 1)c_{55} + c_{33})m_{j-k} + \lambda_m(2 - \lambda)c_{35}l_{j-k}]\hat{C}_k^{(im)}$$
$$+(\lambda_m - 1)[(c_{35} - c_{15})l_{j-k} - (c_{13} + c_{55})o_{j-k}](k + 1)\hat{A}_{k+1}^{(im)}$$
$$+\left[\lambda_m(\lambda_m - 1) \times \left(c_{15}m_{j-k} + c_{35}n_{j-k} - \frac{(c_{13} + c_{55})}{2}l_{j-k}\right)\right.$$
$$\left.+\lambda_m\left(c_{15}n_{j-k} + c_{35}m_{j-k} + \frac{(c_{13} + c_{55})}{2}l_{j-k}\right)\right]\hat{A}_k^{(im)}$$
$$+(\lambda_m - 1)[(c_{34} - c_{56})l_{j-k} - (c_{36} + c_{45})o_{j-k}](k + 1)\hat{B}_{k+1}^{(im)}$$
$$+\left[\lambda_m(\lambda_m - 1) \times \left(c_{56}m_{j-k} + c_{34}n_{j-k} - \frac{(c_{36} + c_{45})}{2}l_{j-k}\right)\right.$$
$$\left.+\lambda_m\left(c_{56}n_{j-k} + c_{34}m_{j-k} + \frac{(c_{36} + c_{45})}{2}l_{j-k}\right)\right]\hat{B}_k^{(im)}\right\}. \tag{9c}$$

Fig. 7. Variation of Re[λ_1] with respect to θ for TiSi$_2$ bodies of revolution having β = 90°, β_1 = 180° under (a) FF and (b) FC boundary conditions.

A close examination of Eq. (9) reveals that the coefficients $\hat{A}_j^{(im)}$, $\hat{B}_j^{(im)}$, and $\hat{C}_j^{(im)}$ for $j \geqslant 2$ in Eq. (8) can be determined by solving the linear algebraic equations in Eq. (9) when $\hat{A}_0^{(im)}, \hat{A}_1^{(im)}, \hat{B}_0^{(im)}, \hat{B}_1^{(im)}, \hat{C}_0^{(im)}$, and $\hat{C}_1^{(im)}$ are known. In other words, Eq. (9) indicate that the coefficients $\hat{A}_j^{(im)}$, $\hat{B}_j^{(im)}$, and $\hat{C}_j^{(im)}$ for $j \geqslant 2$ are functions of $\hat{A}_0^{(im)}, \hat{A}_1^{(im)}$, $\hat{B}_0^{(im)}, \hat{B}_1^{(im)}, \hat{C}_0^{(im)}$, and $\hat{C}_1^{(im)}$. Hence, the solutions to Eq. (6) in sub-domain i of ϕ can be written as

$$\hat{U}_{0i}^{(m)}(\theta, \phi) = \hat{A}_0^{(im)}\hat{U}_{0i0}^{(m)} + \hat{A}_1^{(im)}\hat{U}_{0i1}^{(m)} + \hat{B}_0^{(im)}\hat{U}_{0i2}^{(m)} + \hat{B}_1^{(im)}\hat{U}_{0i3}^{(m)}$$
$$+ \hat{C}_0^{(im)}\hat{U}_{0i4}^{(m)} + \hat{C}_1^{(im)}\hat{U}_{0i5}^{(m)}, \tag{10a}$$

$$\hat{V}_{0i}^{(m)}(\theta, \phi) = \hat{A}_0^{(im)}\hat{V}_{0i0}^{(m)} + \hat{A}_1^{(im)}\hat{V}_{0i1}^{(m)} + \hat{B}_0^{(im)}\hat{V}_{0i2}^{(m)} + \hat{B}_1^{(im)}\hat{V}_{0i3}^{(m)}$$
$$+ \hat{C}_0^{(im)}\hat{V}_{0i4}^{(m)} + \hat{C}_1^{(im)}\hat{V}_{0i5}^{(m)}, \tag{10b}$$

$$\hat{W}_{0i}^{(m)}(\theta, \phi) = \hat{A}_0^{(im)}\hat{W}_{0i0}^{(m)} + \hat{A}_1^{(im)}\hat{W}_{0i1}^{(m)} + \hat{B}_0^{(im)}\hat{W}_{0i2}^{(m)} + \hat{B}_1^{(im)}\hat{W}_{0i3}^{(m)}$$
$$+ \hat{C}_0^{(im)}\hat{W}_{0i4}^{(m)} + \hat{C}_1^{(im)}\hat{W}_{0i5}^{(m)}. \tag{10c}$$

Consequently, the asymptotic solutions in sub-domain i of ϕ are

$$u_r^{(i)}(\rho, \theta, z) = \sum_{m=0}^{\infty}\rho^{\lambda_m}\hat{U}_{0i}^{(m)}(\theta, z) + O(\rho^{\lambda_m+1})$$
$$= \tilde{u}_r^{(i)}(\rho, \theta, z, \lambda_m) + O(\rho^{\lambda_m+1}), \tag{11a}$$

$$u_\theta^{(i)}(\rho, \theta, z) = \sum_{m=0}^{\infty}\rho^{\lambda_m}\hat{V}_{0i}^{(m)}(\theta, z) + O(\rho^{\lambda_m+1})$$
$$= \tilde{u}_\theta^{(i)}(\rho, \theta, z, \lambda_m) + O(\rho^{\lambda_m+1}), \tag{11b}$$

$$u_z^{(i)}(\rho, \theta, z) = \sum_{m=0}^{\infty}\rho^{\lambda_m}\hat{W}_{0i}^{(m)}(\theta, z) + O(\rho^{\lambda_m+1})$$
$$= \tilde{u}_z^{(i)}(\rho, \theta, z, \lambda_m) + O(\rho^{\lambda_m+1}). \tag{11c}$$

Eq. (11) clearly indicate that the asymptotic solution results in stress singularities at $\rho \to 0$ when the real part of λ_m is less than unity. The resulting order of the stress singularities is Re[λ_m] − 1. When λ_m is a real number smaller than one, the resulting stresses monotonically approach infinity as $\rho \to 0$. When λ_m is a complex number whose real part is less than one, the resulting stresses approach infinity in an oscillating manner as $\rho \to 0$.
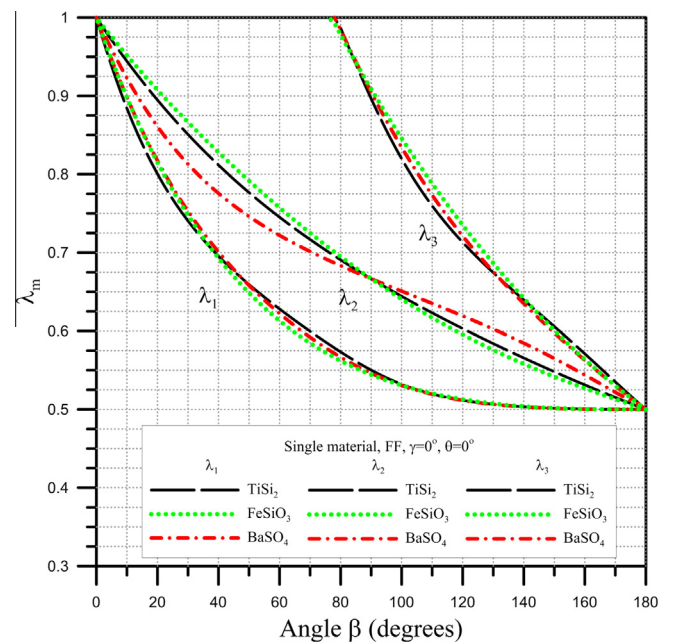

Fig. 8. Variation of λ_m at θ = 0° with respect to β for TiSi$_2$, FeSiO$_3$, and BaSO$_4$ bodies of revolution having β_1 = 180° and FF boundary conditions.

If n sub-domains, as presented in Fig. 3, are used to construct the asymptotic solution for the whole domain of ϕ, then $6n$ coefficients, $\hat{A}_0^{(im)}$, $\hat{A}_1^{(im)}$, $\hat{B}_0^{(im)}$, $\hat{B}_1^{(im)}$, $\hat{C}_0^{(im)}$, and $\hat{C}_1^{(im)}$ for $i = 1, 2, \ldots, n$, must be determined. The traction and displacement continuity conditions between pairs of adjacent sub-domains must be satisfied, yielding $6(n-1)$ equations. Homogenous boundary conditions at $\phi = \phi_0$ and $\phi = \phi_n$ yield another six equations. As a result, $6n$ homogeneous algebraic equations are obtained, requiring $6n$ coefficients to be determined. A nontrivial solution for the coefficients is given by a $6n \times 6n$ matrix with a determinant of zero. The roots of the zero determinant (λ_m), which can be complex numbers, are obtained herein using the numerical method of Müller (1956).

3. Verification of solution

To verify the correctness of the proposed solutions, convergence studies of λ_1 were conducted for bodies of revolution having α ($= \beta + \beta_1$ in Fig. 2) =270° and 360° and with traction-free conditions at $\phi = 0°$ and $\phi = \alpha$. Table 2 shows the results of λ_1 for an isotropic body of revolution with $\alpha = 270°$ and Poisson's ratio $\upsilon = 0.3$, while Tables 3 and 4 show the results for orthotropic bodies of revolution having $\alpha = 360°$ and 270°, respectively. The orthotropic bodies are made of titanium disilicide (TiSi$_2$), which is extensively used in the gate, source and drain contacts in ultra-large-scale integration technology (Özcan et al., 2002).
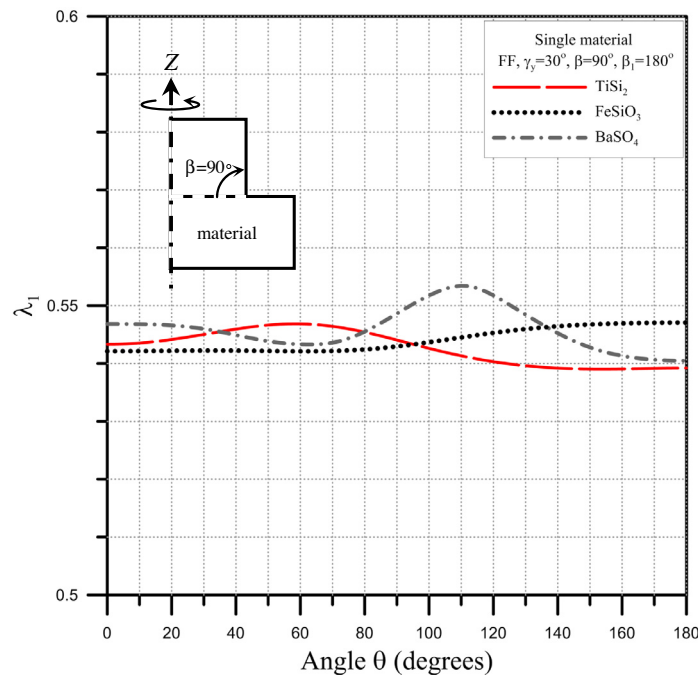
(a)
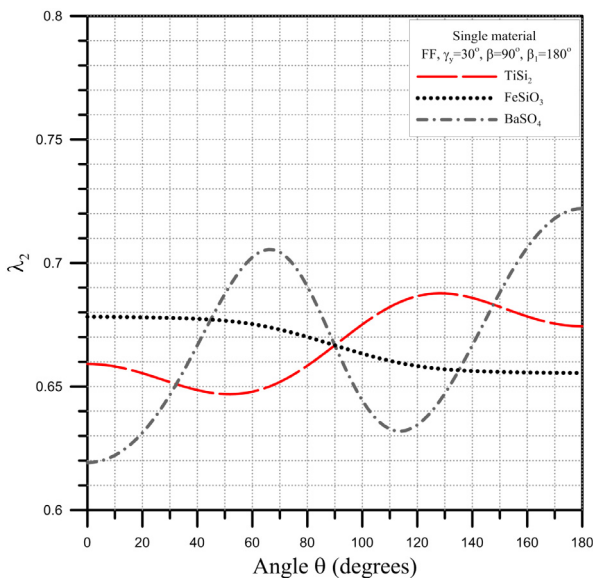
(b)
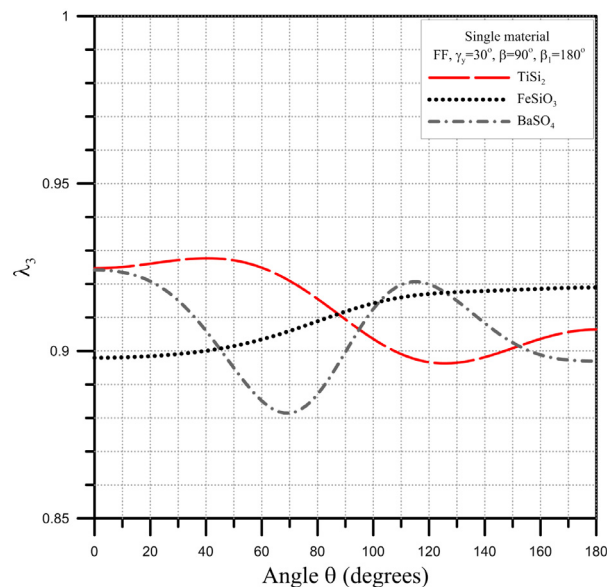
(c)

Fig. 9. Variation of λ_m with respect to θ for TiSi$_2$, FeSiO$_3$, and BaSO$_4$ bodies of revolution having $\beta = 90°$, $\beta_1 = 180°$, and $\gamma_y = 30°$ under FF boundary conditions.

Two different cases, Cases I and II, are considered in Tables 3 and 4. They involve different relations between the geometry coordinate system X–Y–Z and the material coordinate system $\bar{X}$–$\bar{Y}$–$\bar{Z}$, which is used to specify the material properties given in Table 1. In Case I, these two coordinate systems are identical, and in Case II, the Y- and $\bar{Y}$-axes are coincidental and $\bar{X}$–$\bar{Y}$–$\bar{Z}$ is formed by rotating X–Y–Z about the Y-axis through an angle γ_y of 30°. The results were obtained for λ_1 at $\theta = 0°$ and 30° in Cases I and II, respectively.

The present results given in Tables 2–4 were obtained using 2, 4, 8, and 10 equal sub-domains in ϕ in conjunction with 2, 4, 8, 12, and 16 polynomial terms in the series solutions for each sub-domain. These results indicate that convergent results can be obtained by increasing the number of sub-domains or polynomial terms. The convergence of the results can be in an oscillating manner as the number of sub-domains or polynomial terms increases. Table 2 shows that the present results converge to the value of λ_1 determined from the closed-form characteristic equations developed by Huang and Leissa (2007) for an isotropic body of revolution.

The commercial finite element package ABAQUS was also utilized in the analysis of orthotropic bodies of revolution under uniform traction (σ_0) in the Z-direction on the surfaces Z = ± h/2, where h is the height of the body of revolution. Herein, h is set to 20 m and the radii of the surfaces Z = 0 and Z = −h/2 are 5 m and 10 m, respectively. Finite element models of the bodies of revolution were constructed with fine meshes, and very fine meshes were employed near the singular points. Fig. 4 shows the mesh for the bodies with α = 360°. Three-dimensional elements, 20-node quadratic brick elements (C3D20), were used in the analyses. Fig. 5 demonstrates that (σ_{zz}/σ_0) varies with (ρ/R) on the lines (Z,θ) = (0,0°) and (Z,θ) = (0,30°) in Cases I and II, respectively. The straight lines in Fig. 5 were determined from the data points with $\log(\rho/R) \leqslant -3$ using a conventional least-squares method. The slopes of these lines are related to λ_1 by $\lambda_1 = 1 + s$, where s denotes the slope. Similarly, the values of λ_1 were obtained for the bodies of revolution with α = 270°. Tables 3 and 4 reveal that the present results converge to values that agree very well with those determined using ABAQUS.

4. Numerical results and discussion

After the correctness of the presented solutions was verified, the above described method was further applied to determine the roots of λ_m, which are affected by the material properties, configurations of bodies of revolution and the inconsistency between the material coordinate system $\bar{X}$–$\bar{Y}$–$\bar{Z}$ and the geometric coordinate system X–Y–Z. Three orthotropic materials are considered in this study, TiSi$_2$, BaSO$_4$, and FeSiO$_3$, whose material properties are given in Table 1. The configuration of a body of revolution is specified by two parameters, β and β_1, which are defined in Fig. 2. The boundary conditions considered here are simply specified by two letters. The first and second letters refer to the boundary conditions at $\varphi = \varphi_0$ and $\varphi = \varphi_n$, respectively. Free traction and clamped boundary conditions are denoted by F and C, respectively. When the differences between $\bar{X}$–$\bar{Y}$–$\bar{Z}$ and X–Y–Z are considered, $\bar{X}$–$\bar{Y}$–$\bar{Z}$ is assumed to be obtained by rotating X–Y–Z either about the Y-axis through an angle γ_y or about the X-axis through an angle γ_x. The case in which $\bar{X}$–$\bar{Y}$–$\bar{Z}$ and X–Y–Z are identical is denoted by $\gamma = 0°$. The results shown here were obtained using eight equal sub-domains for φ and 12-term series solutions for each sub-domain.

4.1. Single orthotropic material

Fig. 6 plots the variation of λ_1 at $\theta = 0°$ with respect to β for bodies of revolution that are made of TiSi$_2$ or Si under different boundary conditions (FF, FC, and CC). The Young's modulus and Poisson's ratio of Si are E = 130 GPa and $\upsilon = 0.28$, respectively. Notably, the orthotropic bodies of revolution have material coordinates coincident with the geometric coordinates. The roots of λ_1 are all real. Fig. 6 clearly indicates that FC boundary conditions produce the strongest stress singularities among the three combinations of boundary conditions. In general, λ_1 decreases as β increases. Under FC boundary conditions, the values of λ_1 for an orthotropic body of revolution made of TiSi$_2$ do not differ significantly from those for an isotropic body made of Si. Nevertheless, under FF and CC boundary conditions, the strength of stress singularities in a TiSi$_2$ body may or may not be more severe than that in a Si body, depending on the values of β.

Fig. 7 indicates the effects of θ on the orders of the stress singularities in TiSi$_2$ bodies of revolution with $\beta = 90°$ and $\beta_1 = 90°$ under FF and FC boundary conditions. The material coordinate system $\bar{X}$–$\bar{Y}$–$\bar{Z}$ can differ from the geometric coordinate system X–Y–Z, with $\gamma_x = 30°$, 45° or $\gamma_y = 30°$, 45°. Notably, the order of the stress singularities at $\theta = \theta_0$ equals that at $\theta = 2\pi - \theta_0$, so Fig. 7 plots only the values of λ_1 for $0° \leqslant \theta \leqslant 180°$. Free-free boundary conditions result in a real λ_1. Under FC boundary conditions, λ_1 is real when $\bar{X}$–$\bar{Y}$–$\bar{Z}$ is identical to X–Y–Z, and λ_1 can be complex when γ_x or γ_y is equal to 30° or 45°, depending on θ. For instance, λ_1 is complex for $\gamma_x = 30°$ when $5° \leqslant \theta \leqslant 53°$ and when $127° \leqslant \theta \leqslant 175°$. Fig. 7 reveals no clear trend for the effects of γ_x and γ_y on the orders of the stress singularities. Changing γ_x or γ_y from 0° to 30° and further to 45° may or may not increase the strength of the stress singularities, depending on θ. The variations of Re[λ_1] with both γ_x and γ_y are less than 2.5% under FF boundary conditions, and the variation of Re[λ_1] with θ is less than 1.4%. When FC boundary conditions are considered, the variations of Re[λ_1] with both γ_x and γ_y are less than 5.3%, while the variation of Re[λ_1] with θ is less than 6.1%.

Fig. 8 displays the variations of λ_1, λ_2, and λ_3 at $\theta = 0°$ with respect to β for TiSi$_2$, BaSO$_4$, and FeSiO$_3$ under FF boundary conditions when $\gamma = 0°$ and $\beta_1 = 180°$. These first three roots are real and monotonously decrease with increasing β. The values of λ_2 are more affected by the three materials than those of λ_1 and λ_3. The maximum difference between different values of λ_2 for the bodies made of TiSi$_2$, BaSO$_4$, and FeSiO$_3$ is less than 6.8%.
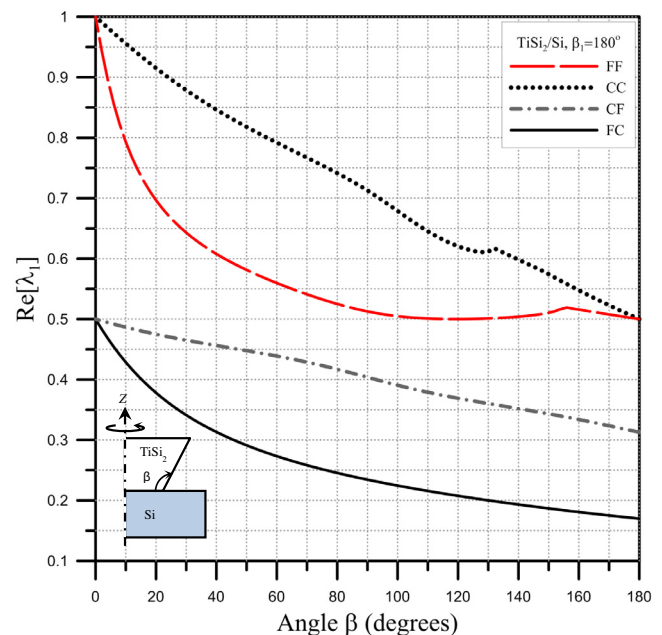

Fig. 10. Variation of Re[λ_1] with respect to β for TiSi$_2$/Si bodies of revolution having $\beta_1 = 180°$ and $\gamma = 0°$ under different boundary conditions.

Fig. 9 depicts the variations of λ_1, λ_2, and λ_3 with respect to θ for TiSi$_2$, BaSO$_4$, and FeSiO$_3$ bodies of revolution with $\beta = 90°$ and $\beta_1 = 180°$ under FF boundary conditions. $\bar{X}-\bar{Y}-\bar{Z}$ is assumed to differ from X–Y–Z, with $\gamma_y = 30°$. Real values of λ_1, λ_2, and λ_3 were found. The body of revolution composed of BaSO$_4$ exhibits the largest variations with respect to θ among the bodies made of the three materials. The variations of λ_1, λ_2, and λ_3 with respect to θ are less than 2.4%, 16.6%, and 4.9%, respectively, for the BaSO$_4$ body of revolution. The maximum variations of λ_1, λ_2, and λ_3 for the TiSi$_2$ and FeSiO$_3$ bodies of revolution are approximately 1.5%, 4.7%, and 3.1%, respectively, and those of the TiSi$_2$ and BaSO$_4$ bodies of revolution are approximately 2.3%, 8.6%, and 4.6%.

4.2. Bi-material anisotropy

This section investigates λ_1 for bi-material bodies of revolution made of Si and TiSi$_2$. Fig. 10 plots the variation of Re[λ_1] at $\theta = 0°$ with respect to β for the bi-material bodies of revolution with $\beta_1 = 180°$ under different boundary conditions (FF, CC, CF, and FC). The portion of the body with $0° \leqslant \phi \leqslant 180°$ is made of Si, whereas the rest is made of TiSi$_2$. $\bar{X}-\bar{Y}-\bar{Z}$ and X–Y–Z are identical. The boundary conditions greatly affect the orders of the stress singularities. Free-clamped boundary conditions yield the strongest stress singularities among the four combinations of boundary conditions under consideration. The relatively abrupt changes around $\beta = 132°$ and $\beta = 155°$ in the curves for CC and FF boundary conditions, respectively, arise from

(a)

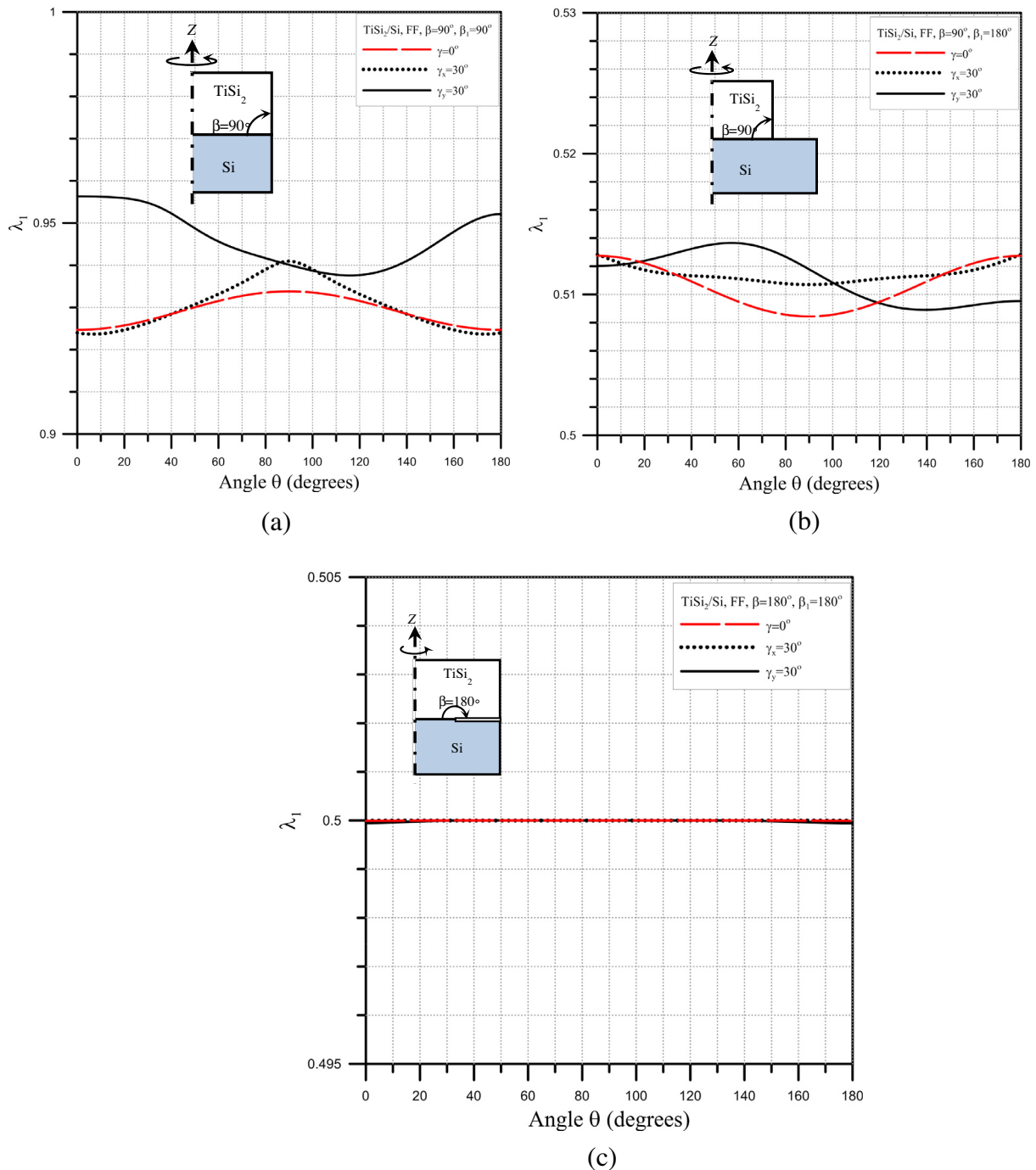
(b)

(c)

Fig. 11. Variation of λ_1 with respect to θ for TiSi$_2$/Si bodies of revolution having $\beta_1 = 180°$ and FF boundary conditions.

the fact that λ_1 changes from real to complex around these two values of β. Comparing Fig. 10 with Fig. 7 reveals that the TiSi$_2$/Si bodies exhibit more severe stress singularities than the TiSi$_2$ bodies under FC and FF boundary conditions when β is less than 180° and 135°, respectively, while the opposite trend is observed under CC boundary conditions when β is less than 180°. The differences in Re[λ_1] between the TiSi$_2$/Si and TiSi$_2$ bodies may reach 14.9%, 12.7%, and 39.2% under FF, CC and FC boundary conditions, respectively.

Fig. 11 shows the variation of λ_1 with respect to θ for bodies of revolution with various geometries under FF boundary conditions. The bodies of revolution again consist of two materials, Si and TiSi$_2$. The figure also displays the shapes and material distributions on a constant θ of the bodies of revolution under consideration. The effects of the inconsistency between $\bar{X}$–$\bar{Y}$–$\bar{Z}$ and X–Y–Z on λ_1 are also studied. Three different relations between $\bar{X}$–$\bar{Y}$–$\bar{Z}$ and X–Y–Z are considered; they are identical ($\gamma = 0°$), or they differ by $\gamma_x = 30°$ or $\gamma_y = 30°$. Fig. 11(a) considers bi-material cylinders with Si in the domain $90° \leqslant \phi \leqslant 180°$. As θ changes, λ_1 varies between 0.924 and 0.933, between 0.924 and 0.941, and between 0.938 and 0.956 for $\gamma = 0°$, $\gamma_x = 30°$ and $\gamma_y = 30°$, respectively. Fig. 11(b) investigates the bodies of revolution with $\beta_1 = 180°$ and $\beta = 90°$ having Si in the domain $0° \leqslant \phi \leqslant 180°$. As θ changes, λ_1 varies between 0.508 and 0.513, between 0.511 and 0.513, and between 0.509 and 0.514 for $\gamma = 0°$, $\gamma_x = 30°$ and $\gamma_y = 30°$, respectively. Fig. 11(c) concerns bodies of revolution with $\beta_1 = 180°$, $\beta = 180°$ and Si in the domain $0° \leqslant \phi \leqslant 180°$. As θ varies, λ_1 remains approximately constant at 0.5 for $\gamma = 0°$, $\gamma_x = 30°$ and $\gamma_y = 30°$.

5. Conclusion

This study presented an asymptotic solution for geometrically induced stress singularities in rectilinearly anisotropic bodies of revolution, taking into consideration the inconsistency between the material coordinate system $\bar{X}$–$\bar{Y}$–$\bar{Z}$ and the geometric coordinate system X–Y–Z. The eigenfunction expansion approach coupled with a power series solution technique was applied to solve the three-dimensional governing equations in terms of displacement components. The solution incorporates no auxiliary functions, such as stress functions or displacement potential. The proposed solution was verified by convergence studies and by comparing the convergent results with those determined from closed-form characteristic equations for an isotropic body of revolution and from using the commercial finite element package ABAQUS for orthotropic bodies of revolution.

The presented solutions were employed to investigate the stress singularities in bodies of revolution comprised of single orthotropic materials (TiSi$_2$, BaSO$_4$, or FeSiO$_3$) and bi-materials (Si and TiSi$_2$). The numerical results indicate that the stress singularities may depend substantially on the geometry of the body of revolution, its boundary conditions, its material properties, the differences between the material and geometry coordinate systems ($\bar{X}$–$\bar{Y}$–$\bar{Z}$ and X–Y–Z), and the angular coordinate variable (θ).These results are very useful for numerical analyses of static and dynamic stresses and of the deformation of a body of revolution with geometrically induced stress singularities. Notably, the dependence of stress singularities on θ can cause great difficulties in evaluating stress intensity factors in real applications. The presented solutions are easily extended to study the stress singularities in cylindrically anisotropic bodies of revolution by properly modifying [c] in Eq. (2).

References

Bogy, D.B., Wang, K.C., 1971. Stress singularities at interface corners in bonded dissimilar isotropic elastic material. Int. J. Solids Struct. 7, 993–1005.

Bogy, D.B., 1972. The plane solution for anisotropic elastic wedge under normal and shear loading. J. Appl. Mech., ASME 39, 1103–1109.

Burton, W.S., Sinclair, G.B., 1986. On the singularities in Reissner's theory for the bending of elastic plates. J. Appl. Mech., ASME 53, 220–222.

Chaudhuri, R.A., Xie, M., 2000. A novel eigenfunction expansion solution for three-dimensional crack problems. Compos. Sci. Technol. 60, 2565–2580.

Chue, C.H., Tseng, C.H., Liu, C.I., 2001. On stress singularities in an anisotropic wedge for various boundary conditions. Compos. Struct. 54, 87–102.

Chue, C.H., Liu, C.I., 2002. Disappearance of free-edge stress singularity in composite laminates. Compos. Struct. 56, 111–129.

Dempsey, J.P., Sinclair, G.B., 1981. On the stress singular behavior at the vertex of a bi-material wedge. J. Elast. 11, 317–327.

England, A.H., 1971. On stress singularities in linear elasticity. Int. J. Eng. Sci. 9, 571–585.

Hartranft, R.J., Sih, G.C., 1969. The use of eigenfunction expansions in the general solution of the three-dimensional crack problems. J. Math. Mech. 19, 123–138.

Hein, V.L., Erdogan, F., 1971. Stress singularities in a two-material wedge. Int. J. Fract. Mech. 7, 317–330.

Huang, C.S., 2002a. Corner singularities in bi-material Mindlin plates. Compos. Struct. 56, 315–327.

Huang, C.S., 2002b. On the singularity induced by boundary conditions in a third-order thick plate theory. J. Appl. Mech., ASME 69, 800–810.

Huang, C.S., 2003. Stress singularities in angular corners in first-order shear deformation plate theory. Int. J. Mech. Sci. 45, 1–20.

Huang, C.S., Leissa, A.W., 2007. Three-dimensional sharp corner displacement functions for bodies of revolution. J. Appl. Mech., ASME 74, 41–46.

Kuo, M.C., Bogy, D.B., 1974. Plane solutions for the displacement and traction-displacement problems for anisotropic elastic wedges. J. Appl. Mech., ASME 41, 197–202.

Müller, D.E., 1956. A method for solving algebraic equations using an automatic computer. Math. Tables Aids Comput. 10, 208–215.

McGee, O.G., Kim, J.W., 2005. Sharp corner functions for Mindlin plates. J. Appl. Mech., ASME 72 (1), 1–9.

Ojikutu, I.O., Low, R.D., Scott, R.A., 1984. Stress singularities in laminated composite wedge. Int. J. Solids Struct. 20 (8), 777–790.

Özcan, A.S., Ludwig, K.F., Rebbi, P., Lavoie, C., Cabral Jr., C., Jarper, J.M.E., 2002. Texture of TiSi$_2$ thin films on Si (001). J. Appl. Phys. 92 (9), 5011–5018.

Pageau, S.S., Joseph, P.F., Biggers Jr., S.B., 1995. A finite element analysis of the singular stress fields in anisotropic materials loaded in anti-plane shear. Int. J. Numer. Methods Eng. 38, 81–97.

Pageau, S.S., Biggers Jr., S.B., 1996. A finite element approach to three-dimensional singular stress states in anisotropic multi-material wedges and junctions. Int. J. Solids Struct. 33 (1), 33–47.

Ping, X.C., Chen, M.C., Xie, J.L., 2008. Singular stress analyses of v-notched anisotropic plates based on a novel finite element method. Eng. Fract. Mech. 75, 3819–3838.

Stroh, A.N., 1962. Steady state problems in anisotropic elasticity. J. Math. Phys. 41 (2), 77–103.

Stolarski, H.K., Chiang, M.Y.M., 1989. On the significance of the logarithmic terms in the free edge stress singularity of composite laminates. Int. J. Solids Struct. 25, 75–93.

Saidi, A.R., Hejripour, F., Jomehzadeh, E., 2010. On the stress singularities and boundary layer in moderately thick functionally graded sectorial plates. Appl. Math. Model. 34 (11), 3478–3492.

Ting, T.C.T., Chou, S.C., 1981. Edge singularities in anisotropic composites. Int. J. Solids Struct. 17, 1057–1068.

Williams, W.L., 1952a. Stress singularities resulting from various boundary conditions in angular corners of plates in extension. J. Appl. Mech., ASME 19, 526–528.

Williams, W.L., 1952b. Stress singularities resulting from various boundary conditions in angular corners of plates under bending. In: Proceedings of First US National Congress of Applied Mechanics. ASME, New York, pp. 325–329.

Williams, M.L., 1952c. Stress singularities resulting from various boundary conditions in angular corners of plates under bending. In: Proceeding of First US National Congress of Applied Mechanics, pp. 325–329.

Williams, M.L., Owens, R.H., 1954. Stress singularities in angular corners of plates having linear flexural rigidities for various boundary conditions. In: Proceeding of 2nd US National Congress of Applied Mechanics, pp. 407–411.

Williams, M.L., Chapkis, R.L., 1958. Stress singularities for a sharp-notched polarly orthotropic plate. In: Proceeding of Third US National Congress of Applied Mechanics. Providence, Rhode Island, pp. 281–286.

Ying, X., Katz, I.N., 1987. A uniform formulation for the calculation of stress singularities in the plane elasticity of a wedge composed of multiple isotropic materials. Comput. Math. Appl. 14, 437–458.

Zak, A.R., 1964. Stresses in the vicinity of boundary discontinuities in bodies of revolution. J. Appl. Mech., ASME 31, 150–152.